

pubs.acs.org/JPCB Article

Specific Ion Solvation and Pairing Effects in Glycerol Carbonate

Published as part of The Journal of Physical Chemistry virtual special issue "Dor Ben-Amotz Festschrift". Andrew E. Eisenhart* and Thomas L. Beck*



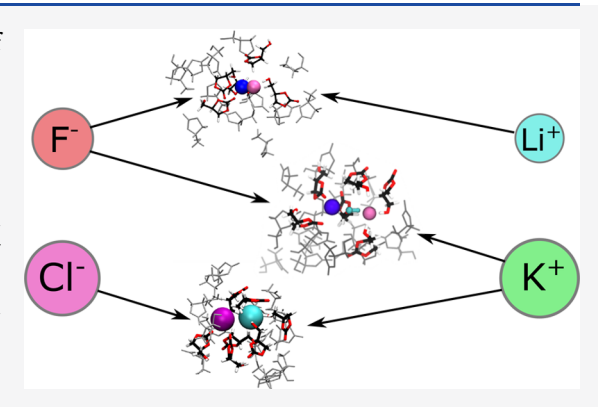
Cite This: J. Phys. Chem. B 2021, 125, 13635–13643



ACCESS

Metrics & More

ABSTRACT: Identifying the driving forces behind the solvation of inorganic salts by nonaqueous solvents is an important step in the development of green solvents. Here we focus on one promising solvent: glycerol carbonate (GC). Using *ab initio* molecular dynamics simulations, we build upon our previous work by detailing glycerol carbonate's interactions with a series of anions, a lithium ion, and the LiF ion pair. Through these investigations, we highlight the changes in solvation behavior as the anion size increases, the competition of binding shown by lithium for the oxygens of GC, and the behavior of the LiF ion pair in a GC solution. These results indicate the importance of the cation's identity in ion-pairing structure and dynamics and lend insight into the key factors behind the specific ion effects seen in GC.



Article Recommendations

1. INTRODUCTION

Glycerol carbonate (4-hydroxymethyl-1,3-dioxolan-2-one or GC, see Figure 1) is a molecule that has attracted recent

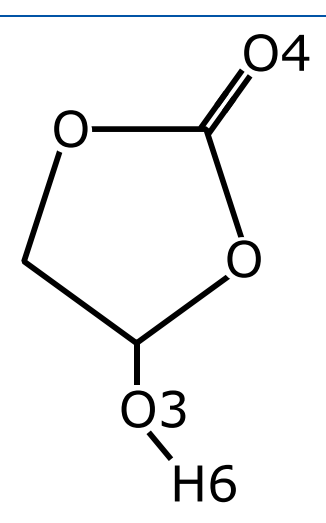


Figure 1. Glycerol carbonate. Several key atoms are labeled.

attention as a green solvent and reactant. As a member of the cyclic carbonate family, GC exhibits many of the same properties as its relatives. Two such relatives, ethylene carbonate and propylene carbonate (EC and PC, see Figure 2), are well-known for their important roles as electrolytes in current energy technologies.^{1–8} Several properties that are shared between the cyclic carbonates promote their usefulness in electrolyte

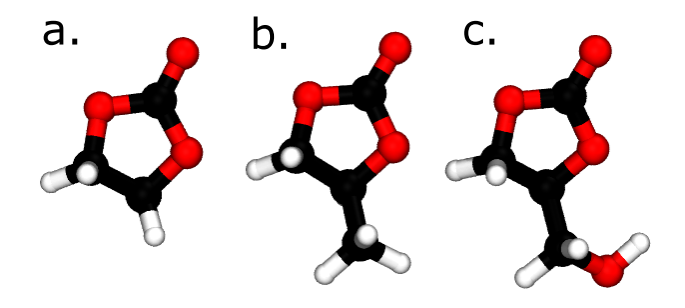


Figure 2. Ethylene (a), propylene (b), and glycerol (c) carbonate.

solutions, ^{9,10} namely, their large dipole moments (4.81, 5.26, and 5.05 D for EC, PC, and GC respectively)¹¹ and dielectric constants (90.5, 66.6, and 111.5).^{12,13} By these criteria, GC appears to show potential as a solvent for inorganic salts in energy storage systems. GC also displays the largest liquid phase temperature range of the cyclic carbonates, with a melting point of -39 °C, a boiling point of 115 °C, and a flash point of 190 °C.

The addition of the hydroxyl group that separates GC from PC also has the effect of increasing the viscosity of the pure GC

Received: July 23, 2021 Revised: November 17, 2021 Published: December 11, 2021





solution to 85.4 cP, an increase of nearly 40× when compared with the values for EC and PC (1.95 and 2.5). We observed in our previous work that this high viscosity originates from the extensive hydrogen bonding that occurs in the pure GC solution. The hydrogen bonding leads to the formation of strongly bound solvent dimers. This stands in contrast to the other cyclic carbonates which exhibit long-range solvent chain formation and in the case of EC long-range bidirectional stacking. 13,14

The strong hydrogen bonding that is present in the pure GC solution has a large impact on its solvation behavior when electrolytes are introduced. In our efforts to investigate the origin of the solvation behavior seen by the Lo Nostro group ^{13,14} when KF is the electrolyte in a GC system, we found that the strong binding between the anion and the hydroxyl of GC leads to the formation of a uniquely organized shared-solvent ion pair. The ions, when paired in this manner, exert a strong structuring effect on the GC molecules that surround the fluoride ion.

Building upon our previous work, this investigation strives to expand our knowledge of glycerol carbonate (GC) and its ion solvation behaviors. 15 We focus on achieving two goals. The first goal is to expand our investigation into GC's interactions with monovalent ions, including the energy-storage relevant Li+ ion, and two anions not previously studied (Br and I). This new work allows us to examine the solvent trends that correlate with ion size and charge density in the halogen family. Our second goal is to quantify the effects of ion pairing on the solvent-ion interactions. In our previous work, we postulated that the identity of the anion was responsible for the shifts in ion-pairing behavior, which in turn influences the increase in the glass transition temperature. 13,14 Other previous works have examined the correlations between ion size and electronegativity or chemical hardness. 16-19 Here, we compare the interactions of KF and KCl as ion pairs and isolated ions. We also introduce the Li⁺ ion into these systems, examining the effect of cation swapping on fluoride's interactions with GC and its pairing behavior. These efforts combine to give us a clearer picture of the dominant interactions in the GC systems and how they can be modified by specific ions.

2. METHODS

In this work, classical molecular dynamics (MD) simulations are performed in the same manner as in our previous study. 15,20 To summarize, the OPLS-AA general force field is implemented by using the GROMACS suite of MD codes to model the solvent and ion interactions. ^{21–23} The particle-mesh Ewald (PME) method is used to model the long-range electrostatic interactions, and long-range energy and pressure corrections are applied to the Lennard-Jones interactions.²⁴ Each isolated ion studied (F⁻, Cl⁻, Br⁻, I⁻, Li⁺, and K⁺) is placed at the center of a unit cell and solvated with 27 glycerol carbonate molecules. Three additional systems containing LiF ion pairs solvated in GC are also created for this study. These ion pairs, to measure ion association, are separated at 2.8, 3.2, or 3.6 Å inside the unit cell (see Figure 3). Position restraints are applied to the solitary and paired ions to preserve their positions throughout the classical simulations. Equilibration is performed by first applying the steepest descent energy minimization algorithm to settle the initial configurations, and then the Nosé-Hoover thermo- $\mathrm{stat}^{25,26}$ is used to raise the system temperature to 300 K. The density is equilibrated at 1 atm pressure with the Parrinello-Rahman barostat.^{27,28} The production runs used as source coordinates for the ab initio molecular dynamics (AIMD) simulations below are run in a constant number/volume/

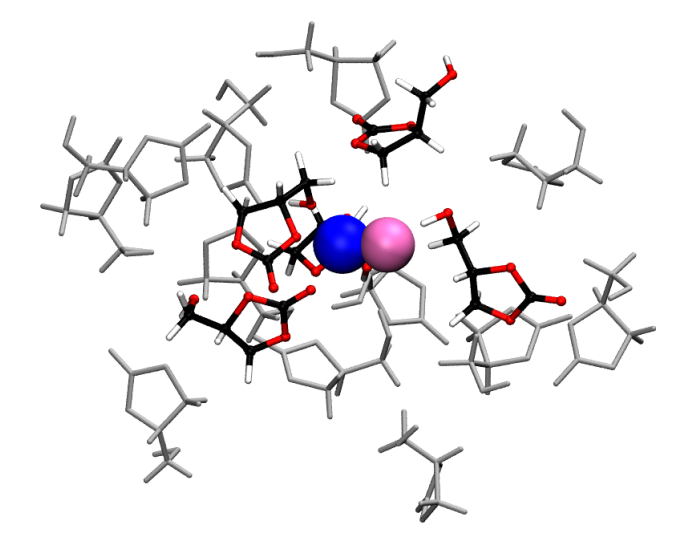


Figure 3. Li (blue)—F (pink) ion pair solvated in glycerol carbonate. The first solvation shell is shown in color. Periodic images have been removed for clarity. The picture was generated by using AIMD simulation data.

temperature (NVT) canonical ensemble for 2 ns, utilizing a 2 fs time step. Equilibrated box side lengths can be found in Table 1.

Table 1. Simulation Box Sizes for the Pressure-Equilibrated Systems

ion	cell length (Å)
F^-	16.51
Cl ⁻	16.83
Br^-	16.84
Γ	16.88
Li ⁺	15.61
K^{+}	16.01

Density functional theory based molecular dynamic simulations are run by using the CP2K package (v2.6.1). ^{29,30} The RevPBE/DZVP-MOLOPT-SR-GTH functional/basis is used in conjunction with the appropriate RevPBE-optimized GTH pseudopotentials. ^{31–35} The D3 dispersion correction with Becke–Johnson damping is included. ^{36,37} The initial coordinates for the AIMD simulations are taken from the previously described equilibrated classical production runs. The total length of each NVT production run is 150 ps. The overall AIMD simulation methodology follows that described in our previous study. ¹⁵

Static DFT calculations are also performed on solvent cluster configurations taken from the AIMD production trajectories (for each anion system). These calculations utilize the hybrid B3LYP functional and def2-TZVP basis set to maximize accuracy and minimize potential basis set superposition error. Through these calculations, the solvation energy, electron affinity, and anion Mulliken charges are obtained for solvation configurations drawn from the AIMD simulations. These calculations closely follow those performed by Bhatt et al., where the interactions of EC with Li⁺ were studied. The chosen geometries for the cluster calculations consist of 100 snapshots. In the AIMD simulations presented here, solvation numbers of 4 and 5 are seen for the fluoride system, while for chloride solvation coordination numbers of 3, 4, and 5 GCs are possible. For both bromide and iodide only three GCs solvate

the anion. The solvation energy $(\Delta E_{\rm solv})$ is calculated via the equation

$$\Delta E_{\text{solv}} = E_{\text{total}}[\text{Anion}(\text{GC})_n] - E_{\text{total}}[\text{Anion}] - nE_{\text{total}}[\text{GC}]$$
(1)

Here E_{total} [Anion(GC)_n] is the total energy of the cluster, E_{total} [Anion] is the energy of the anion by itself, and nE_{total} [GC] is the energy of the GC molecules where n is the solvation number.

To further characterize the electronic structure properties of the anion clusters, we also calculate the forward and reverse electron affinities (noted here as EA_1 and EA_2) via the equations

$$EA_1 = E_{\text{total}}[N+1] - E_{\text{total}}[N] \tag{2}$$

and

$$EA_2 = E_{\text{total}}[N-1] - E_{\text{total}}[N] \tag{3}$$

where $E_{\rm total}[N]$ is the total energy of the cluster at its natural charge of -1, $E_{\rm total}[N+1]$ is the total energy of the cluster with a charge of -2, and $E_{\rm total}[N-1]$ corresponds to a cluster with an overall neutral charge. "N" in these two calculations corresponds to the number of electrons. The calculated forward and reverse electron affinities correlate with the reduction and oxidation potentials of the clusters. ⁴¹ The Mulliken charge analysis and all cluster single point energy calculations were completed with the Gaussian (vg16c01) quantum chemistry software. ^{42,43}

3. RESULTS AND DISCUSSION

3.1. Hydrogen Bonding of Glycerol Carbonate to a Range of Anions. In our previous study, ¹⁵ we found that the primary interactions between fluoride and GC are hydrogenbonding interactions, which are strongest between the H6 hydroxyl tail of GC and the anion. The same interactions between GC and the halogen anion series studied here are displayed via the computed radial distribution functions in Figure 4. It is apparent that the distance of interaction increases and the strength of hydrogen bonding interactions decreases with increasing anion size. This effect is displayed in the RDFs as a shift outward in interaction distance and a reduction in height of the first RDF peak.

As the hydrogen-bonding interactions are reduced and anion size increases, a complex effect on the number of solvent molecules in the first solvation shell is seen. The number of GC molecules that coordinate the fluoride and chloride first solvation shells is near 4. In the case of fluoride, we find that there are two possible states for the first solvation shell. As discussed in our previous work, 4 GCs can interact with fluoride in a tetrahedral geometry. However, during our longer simulations, we also see a 5 GC solvation shell forming temporarily. The formation of this 5-member solvation shell marks the exchange of a new GC molecule into the first solvation shell while another leaves. The strength of the F^- –H6 bonding leads to this transient state being temporarily stabilized. Chloride by comparison exhibits 3 separate and equally possible first solvation structures: the first shell can consist of 3, 4, or 5 GC molecules. The secondary solvation shells of fluoride and chloride both add 3 GC molecules to their local solvation environments.

The two larger anions studied here, bromide and iodide, display solvation patterns similar to one another. They both attract an average of three GC molecules into their first solvation shell and an additional two GC molecules into their second solvation shell. The interactions between the bromide and GC

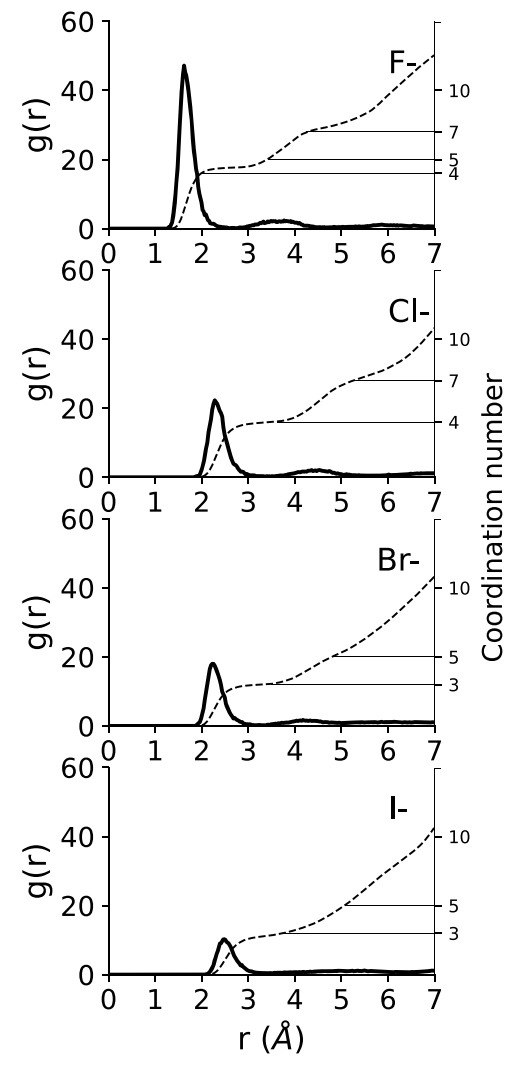


Figure 4. Comparison of GC hydrogen bonding to various unpaired monovalent anions. All RDFs were created by using AIMD simulation data.

hydroxyl tail are slightly stronger than those between iodide and ${\operatorname{GC}}$.

We also examine the polarization occurring in the first solvation shell surrounding each ion. The resulting information is collected in Figure 5. In this graph we can see that in each system the GC molecules in the first solvation shell experience a strong dipole moment enhancement, increasing their dipole moments from the 4.76 and 5.05 D moments calculated for the gas and bulk phases, respectively. (Note that the dipole increase from the gas phase to the pure liquid listed above is much smaller than that seen in the EC and PC liquids. 12 This is due to the very different molecular structural motifs found in the EC/PC and GC liquids. 15) There is a small but noticeable trend in which the dipole moment of GC in the first solvation shell around the ion initially peaks in the fluoride system, decreases in the chloride and bromide system, but increases again in the iodide system. Interestingly, this pattern correlates with the effect of different anions on the glass transition temperature seen by Sarri et al. 14

3.2. Glycerol Carbonate's Binding to Lithium and Potassium. Past studies have quantified the solvation of Li^+ in the similar carbonate solvents EC and PC. ^{12,44} Those studies show that both EC and PC solvate Li^+ by interacting through the carbonyl oxygen (O4 in our labeling scheme). Li^+ binds four

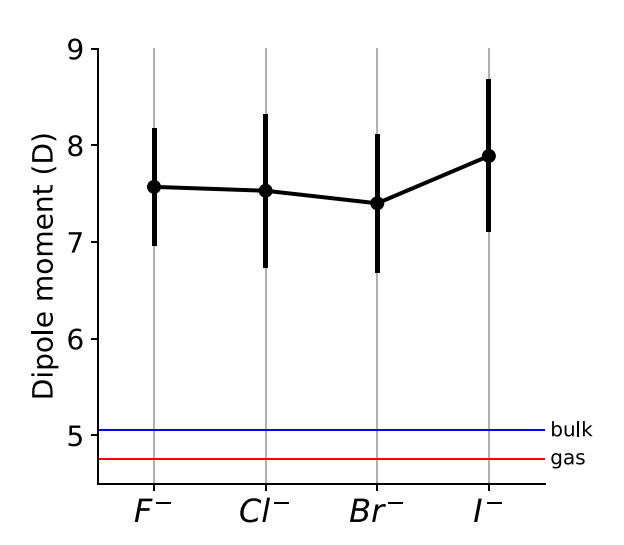


Figure 5. Comparison of GC dipole moment enhancement for the anions. Values correspond to the mean dipole moment of the first solvation shell molecules around the identified ion, and error bars denote the standard deviation. The data are calculated from Wannier centers generated during the AIMD simulations.

solvent molecules in its first solvation shell in both solvents, and these molecules also experience a large dipole moment enhancement.¹²

In Figure 6 we see that the additional oxygen in GC can create competition for binding between the solvent and cations (in contrast with EC or PC). In the case of isolated potassium, the cation strongly prefers to be solvated by the carbonyl (O4) oxygen. See below for a discussion of the impact of anions on the binding preference. Li⁺ by contrast shows clear evidence of competition for binding between the O3 and O4 oxygens. The first solvation shell in the case of Li^+ is still slightly biased toward binding with the O4 oxygen, with an average of three in the first shell. Two further GC molecules interacting through their O3 make up the remainder of the first solvation shell. Li⁺ also displays evidence of a secondary solvation shell consisting of one O3 and one O4, not seen in the potassium system. The stronger binding between the GC molecules and Li+ leads to a more ordered solvation geometry. This can be seen in its narrower GC-cation-GC angle distribution in Figure 7. Because this first solvation shell is a mixture of O4 and O3 ligands, the geometry is difficult to clearly define, but it resembles a trigonal bipyramid with the two associating hydroxyl tails approaching from the top

3.3. Effects of lon-Pairing on Solvent Binding. In this section, we examine the effects that pairing with a counterion has on the solvation characteristics of some of the ions we have previously examined, beginning with the ion pair LiF. After the separate starting simulations reach equilibration, we find that a contact ion pair of LiF is formed (Figure 8).

Similarly to the KCl pair, no bridging hydroxyl tail inserts between the ions to keep them separated. Taking into account the increased interactions between GC oxygens and lithium detailed in Figure 6, we can infer that the effective interactions between the lithium and fluoride ions are stronger than in the KF or KCl pairs. A stronger net attractive force prevents the individual ions from being solvated separately or from forming a shared solvent ion pair like KF. Because the lithium ion shows

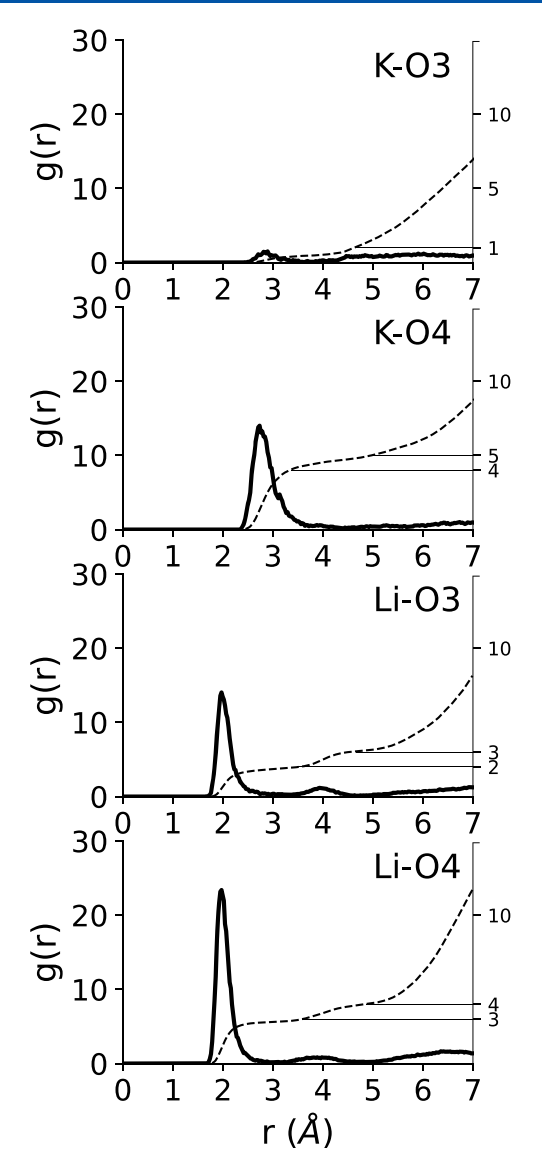


Figure 6. RDFs comparing unpaired cation association with the O3 and O4 oxygens of GC. All RDFs were created by using AIMD simulation data.

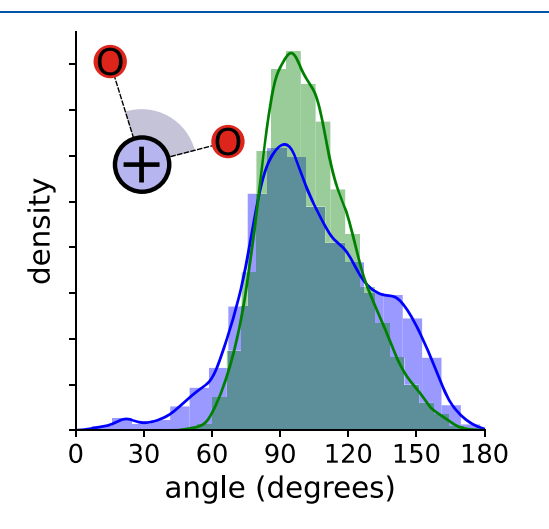


Figure 7. Distributions of the GC-cation-GC angle of the first solvation shell around isolated lithium (green) and potassium (blue) ions.

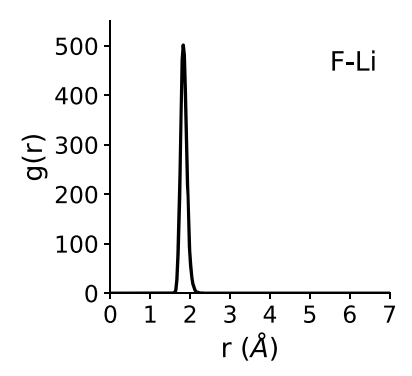


Figure 8. Fluoride—lithium RDF showing the formation of a contact ion pair after equilibration. Data calculated from a combined trajectory consisting of the final 20 ps of each LiF simulation.

significant structuring ability, compared to potassium, it may still have some effect on the glass transition temperature. Further experimental studies investigating the LiF ion pair impact on the $T_{\rm g}$ of GC would allow us to understand which of the two driving forces have more impact on system behavior (the binding strength between the anion and GC or the ability of the ions to form a shared solvent ion pair).

In Figure 9 we show the effect of ion-pairing on the solvation behavior of fluoride and chloride. When isolated, fluoride

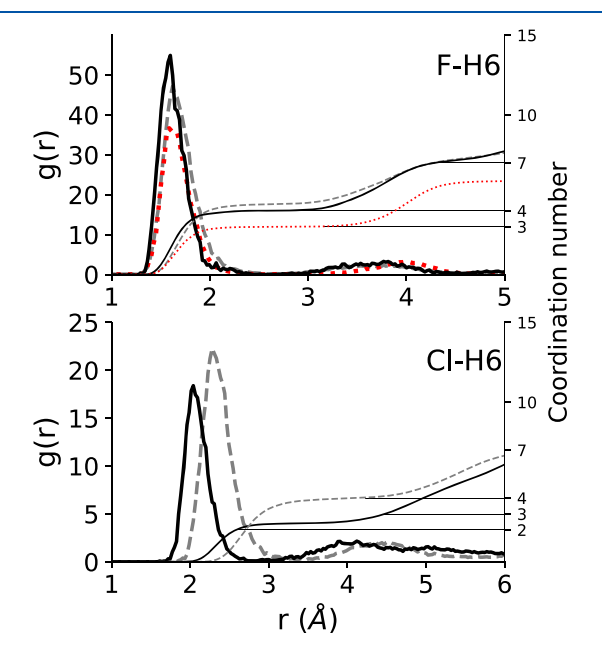


Figure 9. RDFs comparing F^- (top) and Cl^- (bottom) solvation in the presence or absence of a counterion. Paired with K^* : black solid line; paired with Li^* : red dotted line; no counterion: gray dotted line.

displays the potential for a rare transition solvation structure of five GC molecules in its first solvation shell, but when associated with potassium its coordination number lowers to 4. This may imply that a transient solvation structure is less stable or simply that there is less exchange occurring between the first and second shells of fluoride. The reduction in coordination number is accompanied by an increase in the effective free energy of dissociation ($\Delta W_{\rm dissoc}$) for the first solvation shell (see below).

When the fluoride's counterion is lithium, the coordination number of fluoride is reduced to 3. This is also accompanied by a shift outward in the secondary solvation shell. All three states in which fluoride's interactions with GC are studied (isolated, with K^+ , or with Li^+) display a nearly identical first solvation shell distance. The same cannot be said for chloride, however. When chloride associates with the potassium ion, it ejects an average of 1.5 GC molecules. The remaining 2.5 GC molecules, however, are bound closer to the anion. This brings the first peak maximum distance down to 1.81 from 2.3 Å.

The cations can also experience significant solvation changes when paired. Potassium, when paired with fluoride, sees a balancing of its interactions with the O3 and O4 oxygens (Figure 10). This points toward the strong binding of the hydroxyl tail

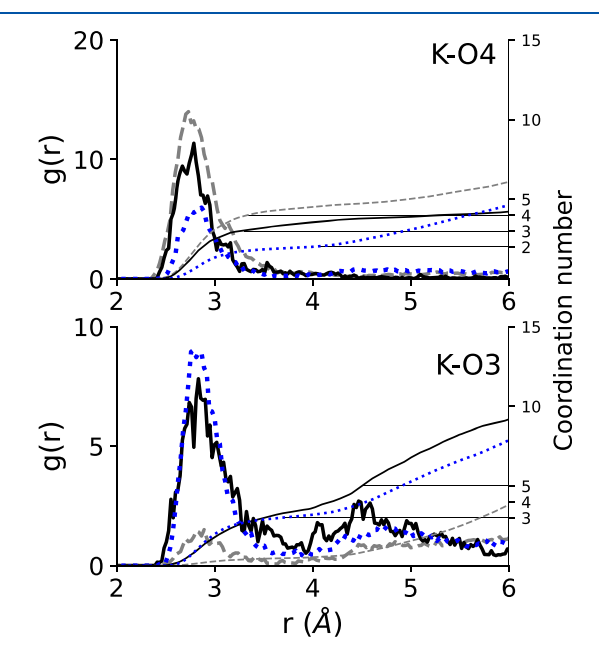


Figure 10. RDFs displaying the effect of a counterion on the solvation of K^+ by the O4 (top) and O3 (bottom) oxygen of GC. Gray dashed line: isolated K^+ ; black solid line: K^+ paired with fluoride; blue dotted line: K^+ paired with chloride.

hydrogen to fluoride as a driving force for attracting the potassium ion toward the O3 oxygen. The resulting structure is a bridging GC that is shared by the K^+ and F^- ions. Potassium also displays stronger binding with the O3 oxygen when paired with chloride.

Lithium, by contrast, binds similarly to the two oxygens of GC. In Figure 11 we can see that the paired Li^+ attracts a smaller total number of GC molecules to the O4 and O3 first solvation shells compared to that of the isolated Li^+ , decreasing the summed coordination number from 5 to 3. This is a result of the formation of the LiF contact ion pair as discussed above. The second peak in the paired Li^+ –O3 RDF can be partially attributed to O3 oxygens which are bound to the fluoride (through the H6 hydrogen). These results show that the lithium ion's interactions with GC are uniformly reduced when paired with fluoride as a result of the counterion's influence and the solvent restructuring.

Table 2 contains the free energy changes ($\Delta W_{\rm dissoc}$) for the process of removing a GC molecule from direct contact with an ion. This free energy change is defined as the difference between the potential of mean force (PMF) values at contact and at large separations (see also Figure 12). The PMF profiles can be used to compute association or dissociation constants for the interaction. The data are assembled for several of the ion—solvent interactions studied here. When we examine

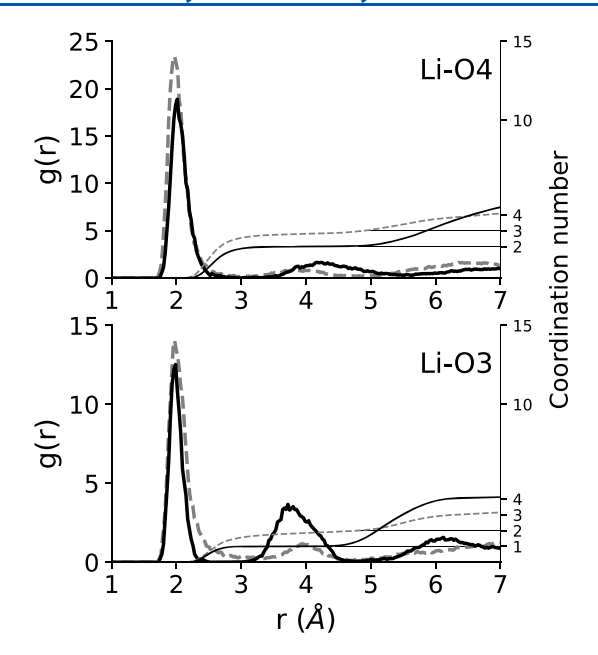


Figure 11. RDFs displaying the effect of a counterion on the solvation of Li^+ by the O4 (top) and O3 (bottom) oxygen of GC. Gray dashed line: isolated lithium ion; black solid line: lithium ion paired with fluoride.

Table 2. Free Energy Change of Dissociation for GC Separating from the Ions Studied^a

ion(s)-GC atom	$\Delta W_{\rm dissoc}$ (kcal mol ⁻¹)	first shell coordination number
FH6	2.1	4.4
Li[F]-H6	2.1	3.0
K[F]-H6	2.3	4.0
Cl ⁻ -H6	1.7	4.0
K[Cl]-H6	1.6	2.4
K+-O4	1.6	4.5
Li^+ -O4	1.9	2.8
K^+ -O3	0.2	0.5
Li^+ -O3	1.6	1.9

"See the definition for $\Delta W_{\rm dissoc}$ in the text and displayed in Figure 12. In the paired species, square brackets denote the ion whose interactions are being measured.

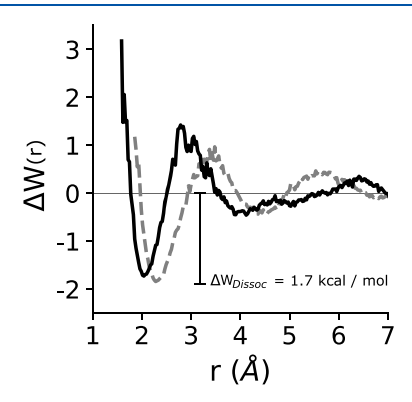


Figure 12. $\Delta W_{\rm dissoc}$ profiles for Cl^- when isolated (gray dashed line) and when paired with K^+ (black solid line). All $\Delta W_{\rm dissoc}$ values are calculated from the anion—H6 pair correlation function shown in Figure 4.

 $\Delta W_{
m dissoc}$ for each of the fluoride systems, we see that, regardless of the ion's pairing status, the value is relatively stable. A

fluoride's $\Delta W_{\rm dissoc}$ when bound with K^+ increases by only 0.2 kcal mol $^{-1}$ compared with that of the isolated fluoride or fluoride bound to Li^+ . Chloride, by contrast, displays a decrease in $\Delta W_{\rm dissoc}$ when paired compared to its isolated state. The magnitude of this decrease, however, is still small. Interestingly, while the $\Delta W_{\rm dissoc}$ for the anions remains stable, their first solvation shell coordination numbers can vary. This indicates that direct hydrogen bonding of the GC to the anion dominates the interactions.

The cation $\Delta W_{\rm dissoc}$ values featured in Table 2 highlight the differences in their binding affinity to the O3 or O4 oxygens. K^+ displays a clear preference for the O4 carbonyl oxygen, with a $\Delta W_{\rm dissoc}$ of 1.6 kcal ${\rm mol}^{-1}$. This is 1.4 kcal ${\rm mol}^{-1}$ larger than its $\Delta W_{\rm dissoc}$ with the O3 oxygen. Li^+ , on the other hand, exhibits a slight preference for the O4 oxygen, but the $\Delta \Delta W_{\rm dissoc}$ between the O3 and O4 oxygens is much smaller at 0.3 kcal ${\rm mol}^{-1}$. The enhanced binding between Li^+ and the O3 oxygen, when compared to K^+ , indicates that the O3 oxygen retains a concentrated negative charge. This allows it to compete with the O4 oxygen when a lithium ion, which also has a concentrated (positive) charge, is solvated by GC.

3.4. Solvation Energies and Charge Transfer in Solvated Anion Clusters. Solvation energies, $\Delta E_{\rm solv}$ (calculated via eq 1), from static DFT calculations are shown in Figure 13 as a function of solvation number. Similar to previous results

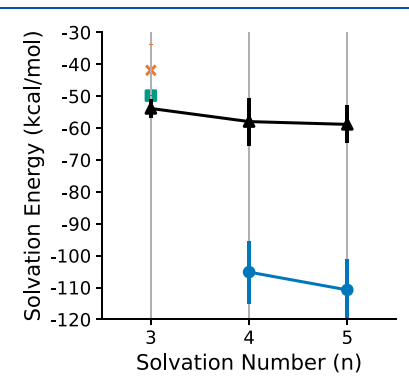


Figure 13. Plot of solvation energy of the four anions studied as a function of solvation number. Markers denote the average value for solvation energy in each system; the error bars denote 1 standard deviation. Fluoride ion: blue with circle markers; chloride ion: black with triangle markers; bromide ion: green with square marker; iodide ion: orange with cross marker.

regarding Li⁺-EC clusters, 40 each system's solvation energy decreases as additional solvent molecules are added to the first solvation shell. However, for the chloride and fluoride systems, the $\Delta \Delta E_{\rm solv}$ values between the 4-solvent and 5-solvent shells are small. In the chloride system, the solvation energies for the 4solvent and 5-solvent clusters are less than 1 kcal/mol apart at -58.0 and -58.8 kcal/mol, respectively. In the two fluoride systems, the average solvation energies are further separated (at -105.2 and -110.7 kcal/mol for the 4-solvent and 5-solvent systems). However, we see that the relatively large error leads to significant overlap of uncertainty between these values. The bromide and iodide 3-solvent clusters exhibit solvation energies (-42.3 and -50.4 kcal/mol) less negative than the corresponding 3-solvent chloride cluster (-54 kcal/mol). This follows our expectations from the RDF results shown above, where the anion solvation energies increase in magnitude as anion size decreases.

To further understand the electronic structure properties of the clusters and how they evolve as the solvation number changes, we have detailed both calculated electron affinities $(EA_1 \text{ and } EA_2)$ in Figure 14.

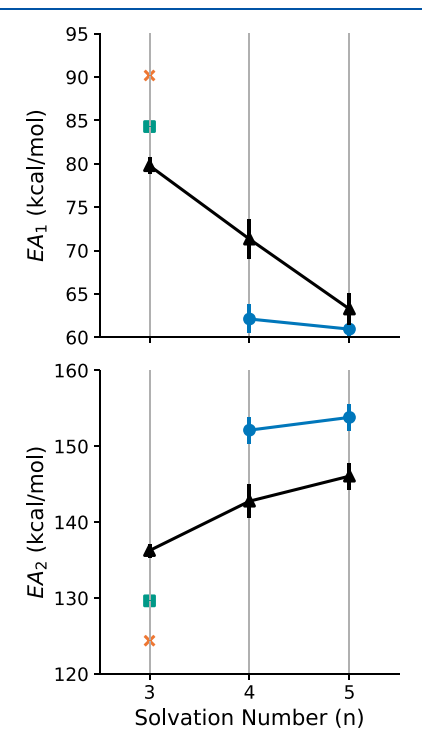


Figure 14. Plot of both electron affinities calculated for the four anions studied as a function of solvation number. Markers denote the average value for the calculated energies in each system. The error bars denote 1 standard deviation. See eqs 2 and 3 for the definitions of EA_1 and EA_2 . Fluoride ion: blue line with circle markers; chloride ion: black line with triangle markers; bromide ion: green with square marker; iodide ion: orange with cross marker.

In Figure 14, we again see trends that track with anion size and "hardness". In the first electron affinity graph (EA_1) , the addition of an electron to any of the clusters (taking them from an overall charge of -1 to -2) results in positive, or unfavorable, electron affinities. The magnitude of this affinity follows the same trend as $\Delta E_{\rm solv}$, with fluoride experiencing the smallest positive EA_1 and iodide the largest. Similar to the solvation energies seen above, the 4- and 5-fluoride-solvent clusters exhibit almost identical EA_1 's. Chloride's EA_1 , however, has a larger dependence on solvent number. This may indicate that the "softer" anion's EA_1 can be more influenced by the surrounding solvent, but further investigation of other anion—solvent clusters is necessary.

The second calculated electron affinity (EA_2) corresponds to the removal of an electron from the clusters, making them neutral. The collected values here, like the values for EA_1 , are large and positive. Each anion system's EA_2 is larger than its corresponding EA_1 value, however, showing that the energy change for removal of an electron from these anion clusters is of larger magnitude than the addition of one. Similar to the progressive trend we see in the EA_1 graph, we again see a trend dependent on anion size. Fluoride clusters have a larger EA_2 than chloride, chloride's EA_2 is larger than bromide, and bromide's EA_2 is larger than iodide's. These trends together show a representation of the effect that the anion's size, "hardness", and electronegativity have on the electronic structure behavior of

these systems. The more electronegative and "hard" fluoride is more resistant to the removal of an electron but more receptive to the addition of one. Adding solvent molecules "softens" the cluster to electron addition but "hardens" it with regard to electron removal.⁴⁷

To finalize our investigation of these anion clusters (and in particular their electronic structure properties), we calculate the partial charge (e) on each of the anions in the studied clusters. These results are displayed in Figure 15.

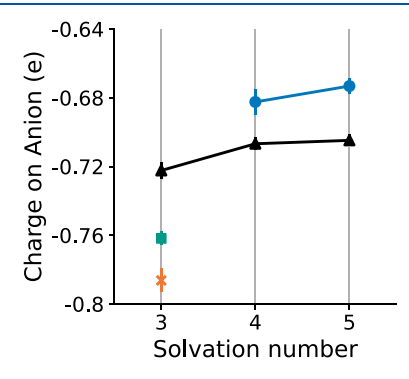


Figure 15. Plot of the Mulliken charge on each of the four anions studied as a function of solvation number. Markers denote the average value for ionic charge in each system. The error bars denote 1 standard deviation. Fluoride ion: blue line with circle markers; chloride ion: black line with triangle markers: bromide ion: green with a square marker; iodide ion: orange with a cross marker.

Interestingly, in these results, we see the opposite of what we might expect from the EA calculations. Instead of fluoride (the "hardest" anion) retaining the most charge of any anion, it donates the most charge to the surrounding solvent. The trend then follows as before, with chloride donating less than fluoride, bromide less than chloride, and iodide least of all. Adding solvent to a cluster increases the overall amounts of charge donated to the solvent, but the amounts donated for both chloride and fluoride systems are very similar for the 4- and 5-solvent systems. This "reversal" of expectations may be a direct result of an increased "chemical" aspect of the binding between the anion and the hydroxyl tail of GC, particularly in the case of fluoride. This chemical aspect of binding increases with anion hardness and electronegativity and correspondingly decreases with anion size.

4. CONCLUSIONS

The aim of this work has been to expand our previous investigations into the ion solvation behavior of glycerol carbonate to the remainder of the halogen chemical family, investigate GC's solvation of lithium, and to further quantify the effect that ion-pairing has on the interactions between the individual ions and GC. These goals were chosen to provide a deeper understanding of GC's specific ion solvation behavior.

When examining the interactions of the isolated anions with GC, we find that there is a clear trend of weaker interactions with the solvent as the anion size increases. In addition, the size increase modifies the coordination numbers in the anion's first solvation shell. The isolated cations also display differences, not only in the strength of their interactions with the solvent but also in their preference for one interaction site or another. Interestingly, both the Li⁺ and K⁺ cations show the same overall coordination number (5) when both interacting oxygens are summed, despite the ion size differences. Investigation into the

solvation geometries of the cations shows that the weaker interactions between the potassium and GC lead to a less ordered and less well-defined first solvation shell geometry when compared to lithium.

For the LiF ion pair, we find that, similar to KCl in our previous work, the two ions form a contact ion pair in GC.¹⁵ This yields insight into the relative strengths of the interactions between the ions. Our study progressed to examine ion-pairing effects on the individual ion-solvent interactions. In the case of fluoride, its interactions with GC are at their greatest when paired with potassium. These interaction changes, combined with the structuring effect of the shared-solvent ion pair on the local solvent, can explain the enhanced stability of the KF ion pair and its impact on the glass transition temperature. In contrast, chloride's interaction energies and local solvation structuring are reduced when paired with potassium. This may explain KCl's lack of impact on the macroscopic properties of GC solutions. 13 From our inferred conclusions regarding the strength of the interaction between Li+ and F-, we anticipate that this ion pair would not have the same impact on the glass transition temperature as KF. The ion-pairing preferences discussed above are reminiscent of Collins' law of matching water affinities (LMWA) that has proven so useful in ion hydration studies. 48 Collins' LMWA has also recently been reformulated as a law of matching solvent affinities in nonaqueous solvents. $^{49-51}$

In the isolated cluster calculations, we shed further light on the nature and magnitude of the solvent-anion interactions. We found that, similar to previous results for Li⁺-EC systems, the optimum number of solvent molecules for an ion can be elucidated by analyzing the solvation energy, electron affinities, and ion charge. Our results from these quantities show that the 4- and 5-solvent clusters for fluoride show relatively similar solvation energies and electron affinities. However, the small size of the fluoride ion makes the chance of seeing the 4-member solvation cluster more likely. The results for the remainder of the anions follows the previously established trends of "hardness" for anions, with the larger, more diffuse anions more likely to accept oxidation and less likely to accept reduction. As the "hardness" and electronegativity of the anions increase, we also observe an increase in the magnitude of the solvation energy. Further investigations of cluster stability could include more thorough evaluations of the solvation free energies utilizing a method such as quasi-chemical theory.⁵²

The above observations shed light on the specific interactions of GC with a broader range of anions and cations. Quantifying the differences in interactions between isolated and paired ions with this solvent gives us insight into how changing the identity of the anion or cation can influence the microscopic and macroscopic behaviors of the system. The next logical step in the investigations of GC should entail the investigations of more complex molecular and multivalent ions.

AUTHOR INFORMATION

Corresponding Authors

Andrew E. Eisenhart — Department of Chemistry, University of Cincinnati, Cincinnati, Ohio 45221, United States; Email: eisenhaw@mail.uc.edu

Thomas L. Beck — Department of Chemistry, University of Cincinnati, Cincinnati, Ohio 45221, United States; Present Address: National Center for Computational Sciences, Oak Ridge National Laboratory, Oak Ridge, TN 37830;

orcid.org/0000-0001-8973-7145; Email: becktl@ucmail.uc.edu

Complete contact information is available at: https://pubs.acs.org/10.1021/acs.jpcb.1c06575

Notes

The authors declare no competing financial interest.

ACKNOWLEDGMENTS

We thank Pierandra Lo Nostro and Barry Ninham for helpful discussions. We are grateful for numerous discussions concerning solvation with Dor Ben-Amotz. This material is based upon work supported by the National Science Foundation under Grants CHE-1565632 and CHE-1955161. The computations were performed at the Ohio Supercomputer Center and the University of Cincinnati Advanced Research Computing Center. 53,54

REFERENCES

- (1) Goodenough, J. B.; Park, K.-S. The Li-Ion Rechargeable Battery: a Perspective. *I. Am. Chem. Soc.* **2013**, *135*, 1167–1176.
- (2) Melot, B. C.; Tarascon, J.-M. Design and Preparation of Materials for Advanced Electrochemical Storage. *Acc. Chem. Res.* **2013**, *46*, 1226–1238
- (3) Choi, N.-S.; Chen, Z.; Freunberger, S. A.; Ji, X.; Sun, Y.-K.; Amine, K.; Yushin, G.; Nazar, L. F.; Cho, J.; Bruce, P. G. Challenges Facing Lithium Batteries and Electrical Double-Layer Capacitors. *Angew. Chem., Int. Ed.* **2012**, *51*, 9994–10024.
- (4) Xu, K. Electrolytes and Interphases in Li-Ion Batteries and Beyond. Chem. Rev. 2014, 114, 11503-11618.
- (5) Xu, K. Nonaqueous Liquid Electrolytes for Lithium-Based Rechargeable Batteries. *Chem. Rev.* **2004**, *104*, 4303–4418.
- (6) Allen, J. L.; Borodin, O.; Seo, D. M.; Henderson, W. A. Combined quantum chemical/Raman spectroscopic analyses of Li+ cation solvation: Cyclic carbonate solvents—ethylene carbonate and propylene carbonate. *J. Power Sources* **2014**, 267, 821–830.
- (7) Borodin, O.; Olguin, M.; Ganesh, P.; Kent, P. R.; Allen, J. L.; Henderson, W. A. Competitive lithium solvation of linear and cyclic carbonates from quantum chemistry. *Phys. Chem. Chem. Phys.* **2016**, *18*, 164–175.
- (8) Cresce, A. V.; Russell, S. M.; Borodin, O.; Allen, J. A.; Schroeder, M. A.; Dai, M.; Peng, J.; Gobet, M. P.; Greenbaum, S. G.; Rogers, R. E.; et al. Solvation behavior of carbonate-based electrolytes in sodium ion batteries. *Phys. Chem. Chem. Phys.* **2017**, *19*, 574–586.
- (9) Peruzzi, N.; Ninham, B. W.; Lo Nostro, P.; Baglioni, P. Hofmeister Phenomena in Nonaqueous Media: The Solubility of Electrolytes in Ethylene Carbonate. *J. Phys. Chem. B* **2012**, *116*, 14398–14405.
- (10) Peruzzi, N.; Lo Nostro, P.; Ninham, B. W.; Baglioni, P. The Solvation of Anions in Propylene Carbonate. *J. Solution Chem.* **2015**, *44*, 1224–1239.
- (11) Chernyak, Y. Dielectric Constant, Dipole Moment, and Solubility Parameters of Some Cyclic Acid Esters. *J. Chem. Eng. Data* **2006**, *51*, 416–418.
- (12) Pollard, T. P.; Beck, T. L. Structure and Polarization Near the Li+ Ion in Ethylene and Propylene Carbonates. *J. Chem. Phys.* **2017**, *147*, 161710.
- (13) Sarri, F.; Tatini, D.; Tanini, D.; Simonelli, M.; Ambrosi, M.; Ninham, B. W.; Capperucci, A.; Dei, L.; Lo Nostro, P. Specific Ion Effects in Non-Aqueous Solvents: The Case of Glycerol Carbonate. *J. Mol. Lig.* **2018**, *266*, 711–717.
- (14) Sarri, F.; Tatini, D.; Ambrosi, M.; Carretti, E.; Ninham, B. W.; Dei, L.; Lo Nostro, P. The Curious Effect of Potassium Fluoride on Glycerol Carbonate. How Salts Can Influence the Structuredness of Organic Solvents. *J. Mol. Liq.* **2018**, 255, 397–405.

- (15) Eisenhart, A. E.; Beck, T. L. Quantum Simulations of Hydrogen Bonding Effects in Glycerol Carbonate Electrolyte Solutions. *J. Phys. Chem. B* **2021**, 125, 2157–2166.
- (16) Kirshnamoorthy, A. N.; Oldiges, K.; Winter, M.; Heuer, A.; Cekic-Laskovic, I.; Holm, C.; Smiatek, J. Electrolyte solvents for high voltage lithium ion batteries: ion correlation and specific anion effects in adiponitrile. *Phys. Chem. Chem. Phys.* **2018**, *20*, 25701–25715.
- (17) Smiatek, J.; Heuer, A.; Winter, M. Properties of ion complexes and their impact on charge transport in organic solvent-based electrolyte solutions for lithium batteries: insights from a theoretical perspective. *Batteries* **2018**, *4*, 62.
- (18) Smiatek, J. Specific ion effects and the law of matching solvent affinities: a conceptual density functional theory approach. *J. Phys. Chem. B* **2020**, 124, 2191–2197.
- (19) Miranda-Quintana, R. A.; Smiatek, J. Beneficial properties of solvents and ions for lithium ion and post-lithium ion batteries: Implications from charge transfer models. *Electrochim. Acta* **2021**, *384*, 138418.
- (20) Abraham, M. J.; Murtola, T.; Schulz, R.; Páll, S.; Smith, J. C.; Hess, B.; Lindahl, E. GROMACS: High Performance Molecular Simulations Through Multi-Level Parallelism from Laptops to Supercomputers. *SoftwareX* **2015**, *1*, 19–25.
- (21) Jorgensen, W. L.; Tirado-Rives, J. Potential Energy Functions for Atomic-Level Simulations of Water and Organic and Biomolecular Systems. *Proc. Natl. Acad. Sci. U. S. A.* **2005**, *102*, 6665–6670.
- (22) Dodda, L. S.; Vilseck, J. Z.; Tirado-Rives, J.; Jorgensen, W. L. 1.14* CM1A-LBCC: Localized Bond-Charge Corrected CM1A Charges for Condensed-Phase Simulations. *J. Phys. Chem. B* **2017**, 121, 3864–3870.
- (23) Dodda, L. S.; Cabeza de Vaca, I.; Tirado-Rives, J.; Jorgensen, W. L. LigParGen Web Server: an Automatic OPLS-AA Parameter Generator for Organic Ligands. *Nucleic Acids Res.* **2017**, *45*, W331–W336.
- (24) Essmann, U.; Perera, L.; Berkowitz, M. L.; Darden, T.; Lee, H.; Pedersen, L. G. A Smooth Particle Mesh Ewald Method. *J. Chem. Phys.* **1995**, *103*, 8577–8593.
- (25) Nosé, S. A Molecular Dynamics Method for Simulations in the Canonical Ensemble. *Mol. Phys.* **1984**, *52*, 255–268.
- (26) Hoover, W. G. Canonical Dynamics: Equilibrium Phase-Space Distributions. *Phys. Rev. A: At., Mol., Opt. Phys.* **1985**, *31*, 1695.
- (27) Parrinello, M.; Rahman, A. Polymorphic Transitions in Single Crystals: A New Molecular Dynamics Method. *J. Appl. Phys.* **1981**, 52, 7182–7190.
- (28) Nosé, S.; Klein, M. Constant Pressure Molecular Dynamics for Molecular Systems. *Mol. Phys.* **1983**, *50*, 1055–1076.
- (29) Borštnik, U.; Van de Vondele, J.; Weber, V.; Hutter, J. Sparse Matrix Multiplication: The Distributed Block-Compressed Sparse Row Library. *Parallel Comput.* **2014**, *40*, 47–58.
- (30) Hutter, J.; Iannuzzi, M.; Schiffmann, F.; Van de Vondele, J. Cp2k: Atomistic Simulations of Condensed Matter Systems. *Wiley Interdiscip. Rev. Comput. Mol. Sci.* **2014**, *4*, 15–25.
- (31) Hartwigsen, C.; Gœdecker, S.; Hutter, J. Relativistic Separable Dual-Space Gaussian Pseudopotentials from H to Rn. *Phys. Rev. B: Condens. Matter Mater. Phys.* **1998**, 58, 3641.
- (32) Goedecker, S.; Teter, M.; Hutter, J. Separable Dual-Space Gaussian Pseudopotentials. *Phys. Rev. B: Condens. Matter Mater. Phys.* **1996**, *54*, 1703.
- (33) Van de Vondele, J.; Hutter, J. Gaussian Basis Sets for Accurate Calculations on Molecular Systems in Gas and Condensed Phases. *J. Chem. Phys.* **2007**, *127*, 114105.
- (34) Krack, M. Pseudopotentials for H to Kr Optimized for Gradient-Corrected Exchange-Correlation Functionals. *Theor. Chem. Acc.* **2005**, *114*, 145–152.
- (35) Perdew, J. P.; Burke, K.; Ernzerhof, M. Generalized Gradient Approximation Made Simple. *Phys. Rev. Lett.* **1996**, *77*, 3865–3868.
- (36) Grimme, S.; Ehrlich, S.; Goerigk, L. Effect of the Damping Function in Dispersion Corrected Density Functional Theory. *J. Comput. Chem.* **2011**, 32, 1456–1465.

- (37) Grimme, S.; Antony, J.; Ehrlich, S.; Krieg, H. A Consistent and Accurate Ab Initio Parametrization of Density Functional Dispersion Correction (DFT-D) for the 94 Elements H-Pu. *J. Chem. Phys.* **2010**, 132, 154104.
- (38) Yanai, T.; Tew, D. P.; Handy, N. C. A new hybrid exchange—correlation functional using the Coulomb-attenuating method (CAM-B3LYP). *Chem. Phys. Lett.* **2004**, 393, 51–57.
- (39) Weigend, F.; Ahlrichs, R. Balanced basis sets of split valence, triple zeta valence and quadruple zeta valence quality for H to Rn: Design and assessment of accuracy. *Phys. Chem. Chem. Phys.* **2005**, *7*, 3297–3305.
- (40) Bhatt, M. D.; Cho, M.; Cho, K. Interaction of Li+ ions with ethylene carbonate (EC): Density functional theory calculations. *Appl. Surf. Sci.* **2010**, 257, 1463–1468.
- (41) Calbo, J.; Viruela, R.; Ortí, E.; Aragó, J. Relationship between electron affinity and half-wave reduction potential: a theoretical study on cyclic electron-acceptor compounds. *ChemPhysChem* **2016**, *17*, 3881–3890.
- (42) Frisch, M. J.; Trucks, G. W.; Schlegel, H. B.; Scuseria, G. E.; Robb, M. A.; Cheeseman, J. R.; Montgomery, A. J., Jr.; Vreven, T.; et al. *Gaussian 03*; Gaussian, Inc.: Wallingford, CT, 2004.
- (43) Mulliken, R. S. Electronic population analysis on LCAO-MO molecular wave functions. I. J. Chem. Phys. 1955, 23, 1833–1840.
- (44) Arslanargin, A.; Powers, A.; Beck, T. L.; Rick, S. W. Models of Ion Solvation Thermodynamics in Ethylene Carbonate and Propylene Carbonate. *J. Phys. Chem. B* **2016**, *120*, 1497–1508.
- (45) Gilson, M. K.; Given, J. A.; Bush, B. L.; McCammon, J. A. The statistical-thermodynamic basis for computation of binding affinities: a critical review. *Biophys. J.* **1997**, *72*, 1047–1069.
- (46) Zhu, P.; Pratt, L.; Papadopoulos, K. Pairing of 1-hexyl-3-methylimidazolium and tetrafluoroborate ions in *n*-pentanol. *J. Chem. Phys.* **2012**, *137*, 174501.
- (47) Miranda-Quintana, R. A. Perturbed reactivity descriptors: the chemical hardness. *Theor. Chem. Acc.* **2017**, *136*, 1–8.
- (48) Collins, K. D. Why continuum electrostatics theories cannot explain biological structure, polyelectrolytes or ionic strength effects in ion–protein interactions. *Biophys. Chem.* **2012**, *167*, 43–59.
- (49) Mazzini, V.; Craig, V. S. Specific-ion effects in non-aqueous systems. *Curr. Opin. Colloid Interface Sci.* **2016**, 23, 82–93.
- (50) Mazzini, V.; Craig, V. S. Volcano plots emerge from a sea of nonaqueous solvents: the law of matching water affinities extends to all solvents. *ACS Cent. Sci.* **2018**, *4*, 1056–1064.
- (51) Miranda-Quintana, R. A.; Smiatek, J. Theoretical Insights into Specific Ion Effects and Strong-Weak Acid-Base Rules for Ions in Solution: Deriving the Law of Matching Solvent Affinities from First Principles. *ChemPhysChem* **2020**, *21*, 2605.
- (52) Beck, T. L.; Paulaitis, M. E.; Pratt, L. R. The Potential Distribution Theorem and Models of Molecular Solutions; Cambridge University Press: Cambridge, 2006.
- (53) Center, O. S. Ohio Supercomputer Center, 1987; http://osc.edu/ark:/19495/f5s1ph73.
- (54) A. R. C. Advanced Research Computing at UC, 2019; https://arc.uc.edu/citing-the-arc/.